Contents lists available at ScienceDirect

Applied Energy

journal homepage: www.elsevier.com/locate/apenergy

Climatic analysis of a passive cooling technology for the built environment in hot countries

John Kaiser Calautit *, Ben Richard Hughes, Diana SNM Nasir

Department of Mechanical Engineering, University of Sheffield, Sheffield S10 2TN, UK

HIGHLIGHTS

- Sub-urban flow simulation was carried out for the analysis of the cooling windcatcher.
- Relevant history and previous works on windcatchers in the UAE were discussed.
- Boundary conditions were varied for each month as per the available climatic data.
- Results of the field testing in RAK carried out in September 2014 were discussed.
- Validation of numerical model using field data showed good agreement.

GRAPHICAL ABSTRACT

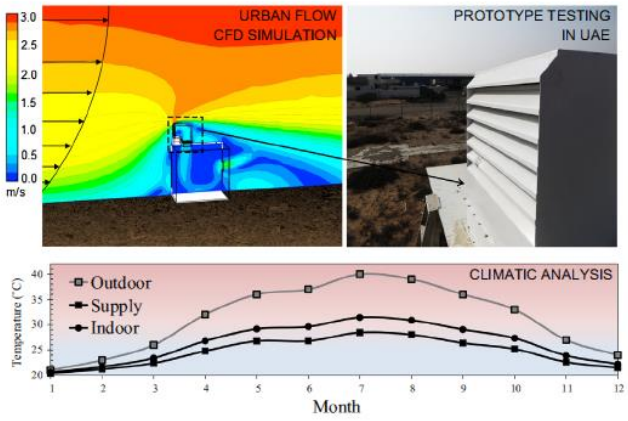

Abstract

The aim of this work was to determine the ventilation and cooling potential of a passive cooling windcatcher operating under hot climatic conditions by replicating the monthly wind velocity, wind direction, temperature and relative humidity (RH) observed in a hot-desert city. The city of Ras-Al-Khaimah (RAK), UAE was used as the location of the case-study and available climatic data was used as inlet boundary conditions for the numerical analysis. The study employed the CFD code FLUENT 14.5 with the standard k-ε model to conduct the steady-state RANS simulation. The windcatcher model was incorporated to a 3 x 3 x 3 m^3 test room model, which was identical to the one used in the field test. Unlike most numerical simulation of windcatchers, the work will simulate wind flows found in sub-urban environment. The numerical model provided detailed analysis of the pressure, airflow and temperature distributions inside the windcatcher and test room model. Temperature and velocity profiles indicated an induced, cooler airflow inside the room; outside air was cooled from 38˚C to 26-28˚C, while the average induced airflow speed was 0.59 m/s (15% lower compared to a windcatcher w/out heat pipes). Field testing measurements were carried out in the Jazira Hamra area of RAK during the month of September. The test demonstrated the positive effect of the integration of heat pipes on the cooling performance but also highlighted several issues. The comparison between the measured and predicted supply temperatures were in good agreement, with an average error of 3.15%.

Keywords: building; computational modelling; field testing; heat pipe; natural ventilation

1. Introduction

Driven by an ever increasing global demand for energy across all aspects of life and industry, carbon emissions have increased at an alarming rate. Governments have been bound to statutory requirements to cut emissions from pre-1990 levels by 80% by the year 2050 [1]. Therefore, a societal movement away from energy intensive processes and the use of new technologies to reduce the energy consumption must be the key focus. The building sector in particular is one of the main end users of energy [2, 3]. Energy consumption for the buildings sector worldwide is expected to grow by 45% in the 2002–2025 period [4]. In rapidly developing Middle Eastern countries such as UAE and Qatar, air-conditioning (AC) is a key contributor to greenhouse gas (GHG) emissions [5]. The extreme conditions of local climate, affordable energy and increased demand for high-levels of comfort had led to the use of energy-intensive AC in nearly all buildings [5]. A study in 2005 [6] indicated that the average consumption per person in Gulf countries was almost 4 times higher than global average.

In addition, the steadily increasing global temperature and decreasing energy security could render the future operation of the built environment un-economical in hot climates, particularly in the Middle East [7]. This could place buildings at risk of over-heating and not habitable during extremely hot periods. It is crucial for buildings to adapt to such situations without the additional energy-intensive mechanical cooling. The answer to the issue, however, might be closer to the Gulf than previously thought. Researchers, engineers and architects are now looking at traditional architecture as a way of providing low-energy cooling [8, 9]. An example of this is the windcatcher or wind tower (Figure 1a), which was used by several Middle East countries for many centuries to capture wind and provide a comfortable indoor environment without using energy [10, 11]. Nowadays, modern version of windcatchers has been implemented in the UK, particularly in schools and offices spaces [12].

Figure 1 (a) A traditional multi-directional wind tower in the Bastakia area of UAE [13] (b) A traditional wind tower with evaporative cooling proposed by Bahadori [10].

The device provides natural ventilation to buildings through wind-driven airflow and thermal effects (buoyancy flows) [14]. Traditionally, wind tower were tall structures which captures wind at higher altitude and wetted clothes were located inside to cool the air supplied to the space below [10]. A different version of a wind tower with evaporative cooling is shown in Figure 1b, which used clay conduits and water spray to cool the air [10]. During night-time,

the wind tower can also provide cooling by "night-flushing" or removing the stored heat in the building fabric. Recently, several studies [15-17] have proposed the addition of heat pipes in windcatchers to enhance its cooling operation and address the issues associated with evaporative cooling method which are detailed in [16]. Figure 2 shows a schematic of the windcatcher with horizontally-arranged heat pipes inside its channel. The system operates by capturing hot outdoor airflow and passing it through one side of the heat pipe arrangement (evaporator), which absorbs the heat and transfer it to a parallel cool sink (condenser). The thermal energy is transferred to the heat pipes in the windcatcher channel where they are cooled as the thermal energy is transferred to the passing airflow. The heat pipe system is based on the continuous cycle of evaporation and condensation process. When heat is applied to the external surface of the heat pipe, the liquid inside the tube boils and vaporises into a gas that moves through the tube seeking a cooler location where it condenses, giving off its latent heat [16]. This will maintain the operating conditions and repeat the cyclic operation of the heat pipe. Adjustable dampers are mounted at the bottom of the unit to control the delivery rate of outdoor air, as fluctuations in external wind speed greatly affect the air movement rate within the occupied space. The heated air is supplied to the room below the channel via the ceiling diffusers. Dampers located downstream of the windcatcher controls the delivery rate of airflow, as fluctuations in outdoor wind greatly influence the supply airflow velocity and temperature [15-16]. The cooled air is supplied to the room beneath the channel via the ceiling diffusers.

Figure 2 (a) 1:1 scale prototype of the passive cooling windcatcher (b) 3D schematic showing the interior of the system.

The objective of this work are two-folds: first, to determine the ventilation and cooling potential of the windcatcher operating under hot climatic conditions by replicating the monthly wind velocity, wind direction, temperature and relative humidity (RH) observed in a hot-desert city such as Ras-Al-Khaimah (RAK), UAE. In our earlier works [15, 16, 18], we've assessed the performance of the windcatcher system based on extreme outdoor conditions (*i.e.* very high outdoor temperature), therefore this study aims to investigate its operation in response to various outdoor conditions. In [15], the authors compared the ventilation and thermal performance of several types of cooling windcatchers; one-sided and multi-directional using CFD modelling. In [16], the ventilation and thermal performance of evaporative cooling and heat pipe-assisted thermal loop for a wind tower in hot conditions were compared using CFD analysis. In addition, two types of heat pipe fluids (ethanol and

water) were also compared using multi-phase CFD modelling. In [18], the authors investigated the ventilation performance of a unidirectional windcatcher using CFD modelling and scaled wind tunnel testing. Experimental results for the indoor and external airflow, supply rate, and pressure coefficients were compared with the numerical results. Smoke visualisation experiment was also conducted to further analyse the detailed airflow structure within the wind catcher and also inside the test room. It is worth noting that previous CFD models were validated using a uniform-flow wind tunnel [14, 18 and 28]. Therefore, simulation of the windcatcher in atmospheric boundary layer (ABL) flow is of further interest. In the current work, we will attempt to simulate approach flows found in an urban scenario which is also essential for the validation of the field study. The second objective is to detail the field testing of the full-scale prototype of the windcatcher in RAK, UAE and analysed the collected field data. Furthermore, the work will use the experimental data to validate the computational method which could be useful for future analysis of windcatcher in urban/sub-urban areas. To the author's knowledge, there is no work that carried out a combined field test–CFD modelling of the thermal performance of a modern windcatcher.

2. Advancement of Wind Towers and Methods

The Baudgeer or traditional wind tower dates back to 1,500 years ago. Their use was spread to Middle East countries such as Iran, Egypt, Jordan, Kuwait and the UAE. The local climate conditions, geographical conditions and social position of the people had a significant role in the design of Baudgeers such as materials, construction, height and number of openings [10]. In the UAE, wind towers can be seen in the town of Bastakiya in the Dubai Creek and signified a remarkable effort to attain comfortable living in a hot climate. Coles *et al.* [13] studied the effectiveness of Dubai's Bastakiya wind towers by carrying out measurement of temperatures, wind tunnel modelling and interviews with previous residents. The work established that wind towers provided a substantial level of comfort during the summer months of the Gulf coast. In an earlier study, Villiers [20] analysed the air temperature and circulation in and around wind towers based on the climate of Abu Dhabi, UAE. The study highlighted the effectiveness of the wind tower in drawing cooler air above the ground level and providing relief from the extreme temperature, particularly during the summer period. Recently, McCabe and Roaf [21] performed dynamic thermal modelling of a Bastakiya house using historical climate data. The study highlighted that like most "climatically effective" historic buildings around the world, the Bastakiya house incorporated a complex and

advanced climatic system which was composed of different elements centered on the wind tower ventilation system. To this end, most of the studies on wind towers in the UAE are mainly based on the traditional systems and many of these historic buildings have been demolished to make way for new developments [20]. The use of modern air-conditioning technology and cheap energy due to government supports have contributed to the diminishing of functional wind towers. Nowadays, wind towers can be seen in new developments in Dubai (Figure 3) which are "e*xaggerated in scale and have no functional purpose*" [22]. Though the "non-functional" wind towers are copies of the ones in historic Bastakiya district, it still shows that there is an awareness of its heritage value. As energy becomes less affordable, energy security decreases and as people become more aware of the environmental impact, the ability to passively cool buildings becomes more important.

Figure 3 Illustrations of "non-functional" wind towers placed on top of buildings in Jumeirah, Dubai, UAE for aesthetic purposes [22].

Many researchers [8] have attempted to improve the effectiveness of wind towers by increasing the ventilation rates and operation time. Bahadori [10] was one of the first to investigate the performance of the Baudgeer by analytical and experimental methods. The study introduced new types of systems; Baudgeer with *wetted columns* (un-glased ceramic conduits, see Figure 1) and with *wetted surfaces* (series of straws). Saffari and Hosseinnia [23] used CFD modelling to analyse the cooling potential of a wind tower with wetted curtains inside the channel. The results showed that a 10m wetted curtain was capable of reducing the ambient airflow temperature by 12°C. Bouchahm *et al.* [24] developed a mathematical model to assess several modifications to the Baudgeer to increase its thermal performance. Kalantar [25] used CFD modelling to evaluate the performance of a wind tower with a water spray. The influence of numerous parameters such as the height of tower, materials, vaporised water and environmental factors was investigated. A recent study [26] presented a case study of the design and construction of down-draught cooling wind towers for semi-open courtyards. Several researchers [27-30] focused on the aerodynamics design and ventilation performance of wind towers and its components.

Although the addition of heat pipes in windcatchers for enhanced cooling was recently introduced [15, 16], earlier studies such as [31] have already demonstrated the capabilities of heat pipes for recovering heat in stack ventilation in temperate climates. The work [31] concluded that the pressure loss was minimal and did not impede the flow of the stack system.

The review of current literature showed that significant research interest has been focused on a number of areas relating to the development of windcatcher technology [8-14, 27-30] and its integration with cooling methods [23-26] such as heat pipes [15-18]. The research gaps that this study aims to address are the following; (1) There are limited studies on the experimental investigation of commercial windcatchers, particularly using field test method. (2) Experimental field-testing of windcatchers in hot climates are limited to the traditional systems, for example the works of [8, 10, 14]. (3) Experimental studies on windcatchers with cooling are limited to the evaporative cooling systems [10, 14]. (4) Windcatchers with heat pipes were assessed in previous works [15-16, 18] primarily using CFD modelling and therefore, experimental analysis is of further interest. (5) Most numerical simulation studies of windcatchers have used uniform flow profile as inlet condition. In the current work, approach flows found in an urban scenario (atmospheric boundary layer flows) will be employed. (6) To the author's knowledge, there is no work that carried out a combined field test–CFD modelling of the thermal performance of a commercial windcatcher. (7) Analysis of windcatchers in the UAE region is limited [9, 21].

3. Numerical Methodology

ANSYS FLUENT 14.5 software [33] was used to conduct the steady-state Reynolds averaged Navier–Stokes equation (RANS simulation) which employed a control-volume-based technique for solving the flow equations. The standard *k-ε* turbulence model was used, which is a well-established method in research on natural ventilation [8]. Second-order upwind scheme was used to discretise all the transport equations. The numerical code used the semi-Implicit method for pressure-linked equations (SIMPLE) algorithm for the velocity-pressure coupling of the computation. The governing equations for the conservation of mass (eqn.1), conservation of momentum (eqn.2), conservation of energy (eqn.3) and the transport equations for the turbulence model (eqn.4 and 5) are detailed below:

$$\frac{\partial \rho}{\partial t} + \nabla \cdot (\rho u) = 0 \tag{1}$$

In eqn. 1, ρ is density, t is time and u refers to fluid velocity vector.

$$\frac{\partial (\rho u)}{\partial t} + \nabla \cdot (\rho u u) = -\nabla \mathrm{p} + \rho \mathrm{g} + \nabla \cdot (\mu \nabla u) - \nabla \cdot \tau_t \tag{2}$$

In eqn. 2, p is the static pressure; ρg is the gravitational body force, μ is the molecular viscosity and τ_t is the divergence of the turbulence stresses which accounts for auxiliary stresses due to velocity fluctuations.

$$\frac{\partial(\rho e)}{\partial t} + \nabla \cdot (\rho e u) = \nabla \cdot \left(k_{eff} \nabla T\right) - \nabla \cdot \left(\sum_i h_i j_i\right) \quad (3)$$

In eqn. 3, e is the specific internal energy, k_{eff} is the effective heat conductivity, T is the air temperature, h_i is the specific enthalpy of fluid and j_i is the mass flux.

$$\frac{\partial(\rho k)}{\partial t} + \nabla \cdot (\rho k u) = \nabla \cdot \left[\alpha_k \mu_{eff} \nabla k\right] + G_k + G_b - \rho_\varepsilon \quad (4)$$

$$\frac{\partial(\rho \varepsilon)}{\partial t} + \nabla \cdot (\rho \varepsilon u) = \nabla \cdot \left[\alpha_\varepsilon \mu_{eff} \nabla \varepsilon\right] + C_{1\varepsilon} \frac{\varepsilon}{k}(G_k + C_{3\varepsilon} G_b) - C_{2\varepsilon} \rho \frac{\varepsilon^2}{k} \quad (5)$$

In eqn. 4 and 5, G_k represents the generation of turbulent kinetic energy (TKE) due to average velocity gradients, G_b is source of turbulent kinetic energy due to buoyancy force, α_k and α_ε are turbulent Prandtl numbers, $C_{1\varepsilon}$, $C_{2\varepsilon}$ and $C_{3\varepsilon}$ are empirical model constants.

3.1 Geometry and computational domain

The windcatcher (Figure 3) and test room geometry were created using the Solid Edge CAD software. The same method [14, 28] was applied for importing the CAD solid data into ANSYS DesignModeller (pre-processor) and extracting the fluid domain. The domain (Figure 4) was separated into three parts: the windcatcher, indoor and outdoor environments. The windcatcher was incorporated to the indoor domain with the dimensions of 3 m x 3 m and 3 m, representing a small room. The windcatcher was modelled with seven louvres at the entrance which were all angled at 45° [28]. It was assumed that the windcatcher was supplying airflow at 100 % (fully open); therefore dampers were not modeled explicitly in the system [18]. The door of the test room was not modelled as it was closed-off entirely during the experiment. The dimension (20 mm outer diameter) and spacing (50 mm horizontal and 20mm vertical) of the heat pipes located downstream of the windcatcher channel were based on an earlier study [17, 18], which investigated the velocity and temperature profiles around various heat pipe arrangements to find the optimum for natural ventilation systems. In order to simplify the simulation, the cool sink was not included in the modelling because of the complexity of the current computational domain and the addition of the cool sink would require the use of multi-phase flow modelling. Although this was already carried out in a simple domain such as in a two-way ductwork [16, 17], modelling it inside a very large domain such as the one currently used would be extremely difficult to mesh with required settings, get converge solution, etc. Hence, assumptions were made based on findings of previous works. The cold sink temperature in the previous studies [17, 18] was maintained between 10°C and 20°C. In this study, it was assumed to be maintained at 20°C. It is worth

noting that simulations of the individual heat pipes with combined hot channel and cold channel (cool sink) were carried out in our previous works [17].

Figure 4 CAD model of the windcatcher with cylindrical heat pipes.

Figure 5 shows the computational domain used for the analysis of the test room with a windcatcher. The domain was sufficiently large to prevent artificial acceleration of the flow. The length of the up-stream domain was kept short, 5 times the height of the test room (H = 3 m), to avoid the unintended existence of stream-wise gradients while satisfying the recommendations [32]. The length of the down-stream domain was 15 times the height of test room, sufficiently long to allow the wake region development behind test room, which was important for the simulation of exhaust flow from the leeward opening [32]. In addition, this was also beneficial for the convergence of the solution according to [32] which was observed in Figure 9 and 10. The domain height was 14 times the height of the test room model. Overall, the domain covered a volume of 23H x 21H x 17H. The outdoor domain consisted of an inlet on one side and an outlet on the opposing boundary wall.

Figure 5 Computational domains for the analysis of the windcatcher.

3.2 Computational grid and sensitivity analysis

Due to the complex geometry of the windcatcher model, an unstructured-grid technique was employed to discretise the computational domains [18, 33]. The advanced size function in ANSYS Meshing was used to precisely capture the geometry while maintain a smooth growth rate between regions of curvature [34]. In order to capture accurately the flow-fields near the critical areas of interest (*i.e.* louvers and heat pipes) in the simulation, size functions were applied in those surfaces. The generated computational grid for the windcatcher and room model is displayed in Figure 6. The total number of the grid elements was equal to 5.65 million. The selected resolution of the grid was based on the grid sensitivity analysis (see Figure 7) on several grids and convergence analysis.

Figure 6 Computational grid of test room with windcatcher.

As shown in Figure 7, a grid-sensitivity analysis on three different grids (A, B and C) was performed to show that the grid refinement did not significantly affect the velocity and temperature results [34]. The analysis starts with an initial coarse grid A (4.59 million), and gradually refines it to medium grid B (5.65 million) and then to fine grid C (9.16 million) until the difference between the results were smaller than the acceptable pre-defined error. To have a balance between computational time and accuracy, grid B was selected. It is worth

noting that the computational time for grid A, B and C are approximately 4 hours, 6 hours and 8 hours. The computations were performed using parallel processing on a workstation with one Intel Xeon 2.1 GHz processor and 16GB Fully Buffered DDR2. The velocity and temperature were measured from a point, down-stream of the windcatcher channel.

Figure 7 Grid sensitivity analysis of velocity and temperature from 4.59 to 9.16 million cells.

3.3 Defined boundary conditions

Unlike previous CFD studies on windcatchers [8] which mainly used uniform flow conditions for the inlet, the current work will simulate flows found in an urban scenario. Previous work highlighted the complexity of solving the flow field simulation involved in urban scenarios [35]; however the accuracy can be potentially improved by accounting the effect of urban structures on the atmospheric boundary layer (ABL). Micro-scale simulation effect provides better predictions on the development of the turbulent distribution over urban canopies. The work [36] highlighted the importance of simulating ABL based on the prototype and actual similarities in the conditions.

The boundary conditions were set using the guidelines highlighted by [37] for the simulation of flows in the urban environment. The vertical profiles of the airflow velocity U and TKE k were imposed on the inlet as shown in Figure 5, based on the measurement data of [37]. The mean velocity of the approach flow (Figure 8a) obeyed a power-law with α = 0.25, which corresponds to a sub-urban terrain [37]. It's also worth noting that this was selected based on the observation of the area of the case study in Ras-Al-Khaimah (RAK). For the k-ε model, the values of ε were obtained by assuming local equilibrium of $Pk = \varepsilon$. From Figure 5, the top and side boundaries were defined as *symmetry* and the outlet surfaces of the domain was set as *zero-static pressure*. All the test room surfaces were set as smooth non-slip walls. The standard wall functions were prescribed to the wall boundaries [38]. The wall functions for the ground surface were modified as proposed by [39] to reflect the effect of roughness of the ground using the equivalent sand-grain roughness height k_s and roughness constant C_s.

Figure 8 (a) mean stream-wise velocity U and (b) Turbulence Kinetic Energy (TKE) k of the approaching flow which corresponds to a sub-urban terrain [37F].

In our previous works [15-16, 18], we've investigated the ventilation and thermal performance of the windcatcher system based on extreme outdoor conditions (*i.e.* setting the inlet conditions to 45˚C ambient temperature and low wind speeds). In this work, we aim to determine the ventilation and cooling potential of the windcatcher design operating under hot

climatic conditions by replicating the monthly wind velocity, wind direction, temperature and relative humidity (RH) in the UAE. The field testing of the full scale prototype was carried out in Ras-Al-Khaimah (RAK) therefore; the weather statistics (see Figure 8) for the area was used for the numerical case study. The outdoor airflow temperatures were varied for each month as per the available climatic data and velocity and temperature at the downstream of the windcatcher channel were monitored. The wall temperature of the heat pipes was set between 10-20 °C [17, 18]. As observed in Figure 9, the dominant wind direction for the full year was NNW, hence the opening of the windcatcher was oriented towards the predominant wind. The mean wind speed varied between 3.60 m/s-4.60 m/s throughout the year, this was measure at an elevation of 20m [40]. The lowest mean ambient temperature was during the month of January and highest during July-August. In general, the RH data shows lower RH during summer when more cooling is required and higher during the winter. For simplification, the effect of solar loading was not included in the modelling because it was assumed that there was minimal heat transfer, as the test room was built from highly-insulating materials (see Section 4 for details). The effect of internal heat gains such as the energy released by occupants, equipment, lighting, etc. were also not included in the modelling because the room was empty during the testing period. Internal heat gain due to occupation could have occurred when measurement sensors were being connected or checked, but this was only before and after the test period. Therefore, its effect was considered to be minimal and the room model was assumed to be empty.

Figure 9 (a) Wind and weather statistics for RAK, UAE (b) mean relative humidity from 06/2013 - 09/2015 [40, 41].

3.4 Monitoring and determining solution convergence

Solution convergence is the term for a computational method using iterations to produce a grid solution, whereby the error approaches zero [33]. In FLUENT, solutions are based on iterations against pre-defined convergence criteria which are $1x10^{-6}$ for the energy and $1x10^{-3}$ for all other equations. The residual of an equation at an iteration is compared with the pre-defined or user-specified values. If the residual is less than the user-specified value, that equation is deemed to have converged for an iteration. However, these pre-defined criterions are not suitable for all types of simulations/cases therefore, in addition to monitoring residuals we've also plotted and analysed velocity and temperature results during the solution process. The convergence was monitored and ended when it was assured that further iterations (+2000 iterations) did not yield substantial change in the velocity and temperature

results. In addition to monitoring residuals and solution variables, the property conservation was also checked if satisfied [33]. This was carried out by performing a mass flux balance and heat transfer rate balance for the converged solution. This option was available in the FLUENT flux report panel which allows computation of mass flow rate and total heat transfer rate for the selected boundary zones. For the simulation of wind tower, the mass flow rate balance was below the required value or <1% of smallest flux through domain boundary [33].

4. Experimental Field-Test in the UAE

Field testing measurements were carried out in the Jazira Hamra area of Ras-Al-Khaimah (RAK), which is situated in the northern part of the United Arab Emirates (UAE), located at latitude 25.67 ˚N and longitude 55.78 ˚E with and elevation of 8.00 m. The test location (Figure 10) is within an upscale residential area which includes several housing communities such as the Hamra Village. The climate of RAK can be characterised as a hot-desert climate with very hot summers and mild winters. High temperatures can be expected from June to August, with a mean temperature ranging between 37-40 ˚C as seen in Figure 9. However, due to limited availability of the test facility, the tests were carried out during the month of September (Sept. 17 – 18 of 2014) between 11AM to 4PM. The prevailing winds in RAK are from the northern direction (N-NNW-NW). Therefore, the opening of the windcatcher was positioned to face the predominant wind. The average wind speed in RAK is between 3.60 m/s-4.60 m/s but during the days of test wind speeds went up to about 5.70-6.00 m/s.

The geometry of the design was identical to the numerical model defined in Section 3, except for the small extended part of the roof and the access door. A 1 x 1 m^2 prototype of the cooling windcatcher was manufactured (Figure 2a) and installed on top of an unoccupied 3 x 3 x 3 m^3 test space as displayed in Figure 11. Similarly, the 20mm heat pipes were arranged inside the downstream of windcatcher channel as described in Section 3.1. The cool sink was fed by chilled water every 15 – 20 min at approximately 20 ˚C (varied ±2 ˚C) to maintain the cyclic operation of the heat pipes as described in Section 1. The temperature was maintained by using on-site supply of chilled water.

To minimise heat transfer, the walls and floor of the test room were highly-insulated and built using the following materials: 12 mm gypsum + 60 mm polystyrene foam + 12 mm gypsum which had a *U*-value of 0.130 W/m^2K. The roof was built using the following materials: 30 mm plywood + 60 mm polystyrene foam + 12 mm plywood, which had a *U*-value of 0.120

W/m^2K. In addition, the exterior of the room was also covered with reflective paint. A small cut-out at the back of the room serves as an outlet. The room was empty and the access the door was closed during the entire testing period.

A total of 5 type-k thermocouple was used to measure the temperature of outdoor (1 thermocouple located at a shaded area), supply air (3 equally-spaced thermocouples downstream of windcatcher channel) and heat pipe wall (1 on surface). The thermocouples were all connected to a data logger to monitor and collect the data. The uncertainty associated with the measurement tool was ±0.6 °C at a temperature of 50 °C and ±0.5 °C at 0 °C. This was provided in the manufacturer's calibration certificate but a separate uncertainty analysis was also carried out in the laboratory using a reference thermocouple and a wind tunnel. The measurement device recorded the temperature every second. A weather station within the area provided the data for the wind conditions and also was used to compare the temperature data recorded by the thermocouple for the outdoor.

Figure 10 Location of the test site in RAK, UAE.

Figure 11 (a) Isometric view and (b) side view of the windcatcher mounted on top of the test room.

5. Results and Discussion

5.1 CFD Results

A windcatcher is able to provide ventilation to buildings by the manipulation of pressure differences created by wind flow around a building and the wind tower. This is demonstrated in Figure 12 which shows the distribution of total pressure inside and outside the test room model. As observed, positive pressure is observed near the windward face of the windcatcher; this generates a driving force, forcing airflow through the windcatcher into the test room. Low or negative pressure is produced on the sides and leeward faces of the building due to the airflow moving around these regions. The low or negative pressure areas generate a *suction force*, exhausting air out of the space through the leeward opening as the differences in pressure are attempted to be equalised. Two negative peaks appeared at the top of the windcatcher and at the back wall. It can also be seen that the room was under positive pressure which was parallel with the findings of previous numerical simulations [18]. An average pressure drop of 1.31 Pa was measured across the heat pipe assembly (this is the difference between upstream and downstream total pressure) which is in accordance with the study of [31].

Figure 12 Distribution of the predicted total pressure (P_o).

Figure 13 illustrates the contours of velocity in the vertical plane drawn from the middle of the domain which is aligned with the direction of the flow and contains the centre of the windcatcher with heat pipes. In previous works [14, 18 and 28], simulations were carried out using uniform flow profile as the approach flow. This does not take into account the frictional drag of the ground surface which generates a boundary layer in which there is a progressive reduction in wind speed towards the ground as observed in Figure 13. In addition, the test room in the outdoor domain was also not included, hence this effect was not captured and would also likely affect the simulation of the performance of the windcatcher.

As observed, the wind flow entering from left reduced speed as it approached the windcatcher (from about 2.40 to 1.10 m/s at the height of opening), some of the air entered the windcatcher via the angled louvers and some passed on top or moved around the sides and exited the pressure-outlet boundary. A large recirculation zone with comparatively low airflow velocities was observed in the wake of the test room. After passing the louvers, the airflow that entered the windcatcher was deflected upwards while the lower side of the flow was in reverse which formed a small recirculation region. The flow was observed to be slightly accelerated (up to 1.09 m/s) as it turns sharply inside the 90° corner. Substantial reduction in speed was observed downstream of the heat pipes. The average airflow speed before the heat pipes was 0.67 m/s and average speed after the heat pipes was 0.59 m/s. As mentioned before, the control dampers were not included in the model and were assumed to be fully open. A column of fast moving air (0.45 m/s) enters the space, where the airstream hit the floor of the room and moves toward the opening on the right wall.

Figure 13 Distribution of the predicted velocity magnitude (m/s) for a windcatcher with heat pipes.

As compared to a system without any heat pipes, a distinctly higher airflow can be observed downstream of the windcatcher channel (Figure 14). Measuring the airflow speed at the same location as the previous model, the average was about 0.68 m/s (15% higher than the windcatcher with heat pipes). Overall, a slightly different flow distribution was observed in this study as compared to our previous numerical simulations [18] which could be a result of the use of a different approach flow (based on a sub-urban profile), different mounting location of windcatcher and also the inclusion of the building geometry in the outdoor domain which was not previously considered. Hence, it is important to consider the impact of these factors when performing simulations of windcatchers in urban scenarios.

Figure 14 Distribution of the predicted velocity magnitude (m/s) for a windcatcher without heat pipes.

Figure 15 illustrates the contours of static temperature in the vertical mid-plane which is aligned with the direction of the flow and contains the centre of the windcatcher and heat pipe assembly. The outdoor airflow temperature was set to 38°C to simulate the maximum average in RAK, UAE while using the same flow profile (U_H=2.29 m/s, α=0.25). The CFD model predicted the indoor temperature to be around 26 °C (closer to the air jet) to 30 °C (closer to outlet). A greater temperature reduction was obtained at the immediate downstream of the heat pipes with a supply air temperature between 26 °C (central) - 28 °C (closer to outer walls), a reduction of 10-12 °C. Though the CFD model revealed that the heat pipes had a positive effect on the thermal performance, the temperature inside the room was still above acceptable air temperature levels even for a hot-desert climate [42]. Hence, we propose to resolve this by (a) using a control strategy to optimise/balance the ventilation rate and cooling, (b) conducting parametric optimisation of the windcatcher components particularly the heat pipes and (c) addition of extended surfaces to the heat pipe.

Figure 15 Distribution of the predicted temperature (°C).

Figure 16 shows the effect of various heat pipe operating temperature (10˚C-20˚C) on the supply air temperature. As observed, specifying a lower operating temperature (18˚C-10˚C) further reduced the supply temperature by up 1.2˚C -5.26˚C.

Figure 16 Effect of various heat pipe temperature on thermal performance.

According to the CFD results, the impact of the variation of wind speed in different months on the supply and indoor airflow are summarised in Figure 17a. The measurement planes (equally spaced at 0.33m) that were used to measure the data are shown in Figure 17b. For the supply measurement, a single plane was located downstream of the windcatcher channel and for the indoor measurement, equally spaced planes were drawn inside the room and the collected data were averaged. In general, the airflow supply was higher during the summer months as compared to winter. The average supply velocity varied between 0.63 m/s and 0.82 m/s.

Figure 17 (a) Predicted results for monthly supply and indoor velocity (b) measurement planes for the supply and indoor airflow.

Table 1 displays sample calculation of the supply rates in L/s per occupant and L/s per square area. The Building Regulation's Approved Document F1A [44] recommended that a minimum air supply rate per occupant of 10 L/s per occupant is required for a small

classroom of 15 people [45]. On average, the windcatcher could supply higher than this value for a room with up to 25 occupants.

Table 1 Sample calculations of the supply rates of the windcatcher

Figure 18 shows the predicted monthly supply and indoor air temperature results for the cooling windcatcher using the steady-state model and the climate data of RAK. The highest temperature reduction (11.54 °C) was achieved during the month of July when the mean outdoor temperature was 40 °C and mean wind speed was 4.60 m/s. While the lowest reduction (0.63 °C) was observed during the month of January when the mean wind speed was at 3.60 m/s and the mean outdoor temperature was at 21 °C.

Figure 18 Predicted monthly indoor air temperatures based on RAK weather data. Dashed line represents monthly wind speed (m/s).

Figure 19 displays the predicted monthly supply and indoor relative humidity of air. As expected, the highest increase in relative humidity was observed during summer months when greater reduction in temperature was achieved by the cooling windcatcher. According to CIBSE guide A [43], indoor humidity levels in the range of 40–70% are generally acceptable however, in the context of microbiological growth, the recommended maximum is 60% to minimise the risk of mould growth and dust mites [43]. Hence, more work is required to ensure that this is prevented especially during periods when relative humidity is well above this value (*i.e.* during winter).

Figure 19 Predicted monthly indoor relative humidity based on RAK weather data.

5.2 Field Test Results and Validation

Figure 20 shows the measured outdoor air temperature, supply air temperature at the three positions downstream of the windcatcher (see bottom left of Figure 19) and heat pipe surface temperature during the 5-hour testing on (09/17/14) which started at 11 AM. Wind conditions during the period of the test are also plotted in the graph which shows that the wind was mainly blowing from the south-west direction (the windcatcher was operating as an exhaust at this time) during the first hour. It is worth noting that the windcatcher can operate effectively (as supply) at ±40° wind angle and maximum at ±70° [18]. Based on the positioning of the windcatcher opening which is facing the north-north-west direction, the windcatcher can supply airflow when the wind is blowing between the west and the north-east direction. The measurements for the wind velocity and direction were obtained from the

local weather station with a 1-hour sampling period, which was verified with the available online data [40]. As the windcatcher started to deliver airflow at around 11:40, cool water (at about 20 ˚C) was fed to the cool sink every 15 – 20 min. to maintain the cyclic operation of the heat pipes. From 1 PM and onwards, the wind was blowing within the range of ±40° wind angle and consequently the continuous reduction of supply air temperature. At 1 PM, the wind was predominantly from west-north-west direction and the temperature drop was 4 ˚C-5 ˚C. From 2 to 4 PM, the wind speed increased up to 6 m/s and the temperature drop varied between 3 ˚C–7 ˚C.

Figure 20 Field testing measurements on 09/17/14.

Figure 21 displays the results of the 5-hour testing on (09/18/14) from 11 AM to 4 PM The windcatcher began to deliver airflow into the test room at 11:30 and the temperature drop ranged between 3 ˚C-4 ˚C during this period. Likewise, the wind started to blow consistently within the ±40° wind angle from 1 PM to 4PM and the temperature drop ranged between 3 ˚C–11.5 ˚C during this period.

Figure 21 Field testing measurements on 09/18/14.

Figure 22 shows a detailed view of the temperature measurements from 3 PM to 4 PM. The temperature measurements taken during several periods (03:05, 03:16, 03:30, 03:37, 03:48 and 03:58) were used for the validation of the steady-numerical model. Predicted supply temperatures (+) are added to the chart for comparison with the measured results. As observed, the numerical model in most cases under-predicted the supply temperature, however a similar trend between both methods was observed.

Figure 22 Detailed view of the recorded temperature from 3-4 PM on 09/18/14.

Table 2 summarises the comparison of the measured and predicted supply temperatures detailed above. The average error between the results was 3.15% which could be considered satisfactory considering the limitations of the model and also assumptions used.

Table 2 Comparison between field test data and CFD prediction

6. Conclusion

The aim of this work was to further the research on this technology by determining the ventilation and cooling potential of the windcatcher integrated with heat pipes operating under hot climatic conditions by replicating the monthly wind velocity, wind direction, temperature and relative humidity (RH) observed in a hot-desert city such as Ras-Al-Khaimah (RAK), UAE. The study employed the CFD code FLUENT 14.5 to conduct the

steady-state RANS simulation which employed the Finite Volume Method (FVM) approach. The standard k-ε model was used to model the turbulent nature of the flow. The windcatcher model was incorporated to a 3 x 3 x 3 m^3 test room model which was identical to the one used in the field testing in the UAE. Unlike previous numerical studies on windcatchers which used uniform-flow conditions for the inlet boundary condition, the current work simulated wind flows found in a sub-urban environment. This was carried out by following the best practice guidelines for the simulation of flows in the urban environment which included the use of a computational domain covering a volume of 70 x 63 x 51 m^3.

The numerical model provided detailed analysis of the pressure, airflow and temperature distributions inside the windcatcher and test room model. Based on the pressure analysis, an average pressure drop of 1.31 Pa was measured across the heat pipe arrangement when the outdoor wind speed U_{20m} was set to 3.40 m/s. Under similar conditions, temperature and velocity profiles indicated an induced, cooler airflow inside the room; outside air was cooled from 38˚C to 26-28˚C, while the induced airflow speed was 0.59 m/s on average (15% lower compared to a windcatcher without heat pipes).

The inlet conditions were varied for each month as per the available climatic data and velocity; temperature and humidity at the downstream of the windcatcher channel were monitored. The average supply velocity varied between 0.63 m/s and 0.82 m/s throughout the year. In general, the airflow supply was higher during the summer months as compared to winter. The highest temperature drop (11.54 °C) was achieved during the month of July while the lowest reduction (0.63 °C) was observed during the month of January. Predictions of relative humidity (RH) showed that the highest increase in RH were during the summer months when greater reduction in temperature was achieved by the cooling windcatcher. The increase in RH during winter time were minimal but the values of the outdoor RH were already well above 50% hence, a high indoor RH was observed during winter. Further investigation into the effect of the air temperature reduction and relative humidity on thermal comfort is necessary.

Field testing measurements were carried out in the Jazira Hamra area of Ras-Al-Khaimah (RAK), which is situated in the northern part of the United Arab Emirates (UAE). Although highest temperatures can be expected from June to August, the test was carried out in September (08/17/14-09/17/14) due to limited availability of the test facility. The test demonstrated the positive effect of the integration of heat pipes on the cooling performance

but also highlighted issues which remain to be solved such as the operation of the cool-sink, control strategy and high humidity levels at certain periods. The temperature measurements taken during the following periods; 03:05, 03:16, 03:30, 03:37, 03:48 and 03:58, were used for the validation of the steady-numerical model. The comparison analysis showed that the measured and predicted supply temperatures were in good agreement, with an average error of 3.15%.

Acknowledgement

The support by the University of Sheffield and CSEM (UAE) are gratefully acknowledged. The statements made herein are solely the responsibility of the authors.

Reference

[1] DECC. *Climate Change Act.* London, 2008.
[2] Rahman MM, Rasul MG, Khan MMK. Energy conservation measures in an institutional building in sub-tropical climate in Australia. Applied Energy 2010;87:2994-3004.
[3] Yau YH, Lee SK. Feasibility study of an ice slurry-cooling coil for HVAC and R systems in a tropical building. Applied Energy 2010;87:2699-2711.
[4] Vettorato D, Geneletti D, Zambelli P. Spatial comparison of renewable energy supply and energy demand for low-carbon settlements. Cities 2011;28: 557-566.
[5] Sofotasiou P, Hughes BR, Calautit JK. Qatar 2022: Facing the FIFA World Cup climatic and legacy challenges. Sustainable Cities and Society 2015;14:16-30.
[6] Alnaser WE, Alnaser NW. The status of renewable energy in the GCC countries. Renewable and Sustainable Energy Reviews 2011;15:3074-3098.
[7] Akbari H, Pomerantz M, Taha H. Cool surfaces and shade trees to reduce energy use and improve air quality in urban areas. Solar Energy 2001;79:295-310.
[8] Hughes BR, Calautit JK, Ghani SA. The Development of Commercial Wind Towers for Natural Ventilation: a review. Applied Energy 2011;92:606-627.
[9] Calautit JK, Hughes BR, O'Connor D, Shahzad SS. Numerical and experimental analysis of a multi-directional wind tower integrated with vertically-arranged heat transfer devices (VHTD). Applied Energy 2016.
[10] Bahadori M, Mazidi M, Dehghani AR. Experimental investigation of new designs of wind towers. Renewable Energy 2008;33:2273–2281.
[11] Bouchahm Y, Bourbia F, Belhamri A, Performance analysis and improvement of the use of wind tower in hot dry climate. Renewable Energy 2011;36:898-906.
[12] O'Connor D, Calautit JK Hughes BR.A review of heat recovery technology for passive ventilation applications. Renewable and Sustainable Energy Reviews 2016;54:1481-1493.
[13] Coles A, Jackson P, Jones I. How wind towers work: A study of the effectiveness in Dubai's Bastakiya. International Committee of Vernacular Architecture. Conference at Al Ain, 2012.
[14] Calautit JK, Hughes BR. Measurement and prediction of the indoor airflow in a room ventilated with a commercial wind tower. Energy and Buildings 2014;84:367-377.
[15] Calautit JK, Hughes BR, Chaudhry HN, Ghani SA. CFD analysis of a heat transfer device integrated wind tower system for hot and dry climate. Applied Energy 2013;112,:576-591.

[16] Calautit JK, Chaudhry HN, Hughes BR, Ghani SA. Comparison between evaporative cooling and heat pipe assisted thermal loop for a commercial wind tower in hot and dry climatic conditions. Applied Energy 2013;101:740-755.
[17] Hughes BR, Chaudhry HN, Calautit JK. Passive energy recovery from natural ventilation air streams. Applied Energy 2013;113:127-140.
[18] Calautit JK, Hughes BR, Shahzad SS. CFD and wind tunnel study of the performance of a uni-directional wind catcher with heat transfer devices. Renewable Energy 2015;83:85-99.
[19] Elmualim AA. Effect of damper and heat source on wind catcher natural ventilation performance. Energy and Buildings 2006;38: 939-48.
[20] Villiers MD. Meteorological aspects of the wind towers of the United Arab Emirates. Weather 2003;58:319–324.
[21] Ciaran M, Roaf S.The wind towers of Bastakiya: assessing the role of the towers in the whole house ventilation system using dynamic thermal modelling. Architectural Science Review 2013:56;183-194.
[22] Guardian, An urbanist's guide to Dubai: 'A city too clean for its own good?' Available from: http://www.theguardian.com/cities/2014/may/13/an-urbanists-guide-to-dubai
[23] Saffari H, Hosseinnia S. Two-phase Euler-Lagrange CFD simulation of evaporative cooling in a Wind Tower. Energy and Buildings 2009;41:991–1000.
[24] Bouchahm Y, Bourbia F, Belhamri A. Performance analysis and improvement of the use of wind tower in hot dry climate. Renewable Energy 2011;36:898-906.
[25] Kalantar V. Numerical simulation of cooling performance of wind tower (Baud-Geer) in hot and arid region. Renewable Energy 2009;34:246–254.
[26] Kassir RM. Passive downdraught evaporative cooling wind-towers: A case study using simulation with field-corroborated results. Building Services Engineering Research and Technolog 2015, doi: 10.1177/0143624415603281.
[27] Calautit JK, O'Connor D, Hughes BR. Determining the optimum spacing and arrangement for commercial wind towers for ventilation performance. Building and Environment 2014;82:274-287.
[28] Calautit JK, Hughes BR. Wind tunnel and CFD study of the natural ventilation performance of a commercial multi-directional wind tower. Building and Environment 2014;80:71-83.
[29] Calautit JK, O'Connor D, Sofotasiou P, Hughes B. CFD Simulation and Optimisation of a Low Energy Ventilation and Cooling System. Computation 2015;3:128-149.
[30] Nejat P, Calautit JK, Majid MZ, Hughes BR, Zeynali I, Jomehzadeh F. Evaluation of a two-sided windcatcher integrated with wing wall (as a new design) and comparison with a conventional windcatcher. Energy and Buildings 2016.
[31] Gan G, Riffat SB. A study of heat-pipe heat recovery for natural ventilation. Building Services Engineering Research and Technology 1999;20:57-62.
[32] Franke F, Hellsten A, Schlünzen H, Carissimo B, Best Practice Guideline for the CFD Simulation of Flows in the Urban Environment COST Office, Brussels, 2007.
[33] ANSYS® Academic Research. ANSYS FLUENT User's Guide Release 14.0. Pennsylvania: ANSYS, Inc; 2014.
[34] Chung T. Computational fluid dynamics. Cambridge University Press 2002;1:15-21.
[35] Tsegas G, Moussiopoulos N, Barmpas F, Akylas V, Douros I, An Integrated Numerical Methodology for Describing Multiscale Interaction on Atmospheric Flow and Pollutant Dispersion in the Urban Atmospheric Boundary Layer. Journal of Wind Engineering and Industrial Aerodynamics 2015;144:191-201.
[36] Yuan R, Wu X, Luo T, Liu H, Sun J. A Review of Water Tank Modeling of the Convective Atmospheric Boundary Layer. Journal of Wind Engineering and Industrial Aerodynamics 2011;99:1099-1114.

[37] Tominaga Y, Akabayashi S, Kitahara T.a, Arinami Y. Air flow around isolated gable-roof buildings with different roof pitches: Wind tunnel experiments and CFD simulations. Building and Environment 2015;84:204-213.
[38] Launder BE, Spalding DB. The numerical computation of turbulent flows. Computer Methods in Applied Mechanics and Engineering 1974;3:269–289.
[39] Blocken B, Stathopoulos T, Carmeliet J. CFD simulation of the atmospheric boundary layer: wall function problems. Atmos Environ 2007;41:238–252.
[40] Windfinder, Wind & weather statistics Ras Al-Khaimah Airport, available from: http://www.windfinder.com/windstatistics/ras_al-khaimah_airport
[41] Wundeground, Weather History for Ras Al-Khaimah Airport available from: http://www.wunderground.com/history/airport/OMRK/2015/7/1/MonthlyHistory.html
[42] Dhaka S, Mathur J, Brager G, Honnekeri A. Assessment of thermal environmental conditions and quantification of thermal adaptation in naturally ventilated buildings in composite climate of India. Building and Environment 2015; 86:17-28.
[43] CIBSE Guide A: Environmental Design 2015
[44] Building Regulations 2000: Approved Document F1A: Means of Ventilation 2010, NBS: London.
[45] Building Bulletin, Building Bulletin 98: Briefing Framework for Secondary School Projects, 2004.

Nomenclature and Abbreviations

U	Velocity magnitude (m/s)
T	Air temperature (˚C)
X, Y, Z	Cartesian co-ordinates (m)
Re	Reynolds number
ρ	Air density (kg/m^3)
μ	Kinematic viscosity (m^2/s)
Q	Volume flow rate (m^3/s)
g	Gravitational acceleration (m/s^2)
A	Cross-sectional area (m^2)
ΔP	Total pressure loss (Pa)
P	Pressure (Pa)
P_o	Total pressure (Pa)
P_s	Static pressure (Pa)
L	Length (m)
W	Width (m)
H	Height (m)
t	Time
e	Specific internal energy (J/kg)
k_{eff}	Effective heat conductivity (W/mK)
h_i	Specific enthalpy of fluid
j_i	Mass flux (kg s^{-1} m^{-2})
G_b	Source of turbulent kinetic energy due to buoyancy force
α_k	Turbulent Prandtl numbers
k	Turbulence kinetic energy (m^2/s^2)
ε	Turbulence dissipation rate (m^2/s^3)
α	Power law coefficient
ABL	Atmospheric Boundary Layer

AC	Air-Conditioning
CAD	Computer-aided Design
CFD	Computational Fluid Dynamics
CIBSE	Chartered Institution of Building Services Engineers
FVM	Finite Volume Method
GHG	Greenhouse Gas
RAK	Ras-Al-Khaimah
RANS	Reynolds averaged Navier–Stokes
RH	Relative Humidity
SIMPLE	Semi-Implicit method for Pressure-linked Equations
TKE	Turbulence Kinetic Energy
UAE	United Arab Emirates
UK	United Kingdom

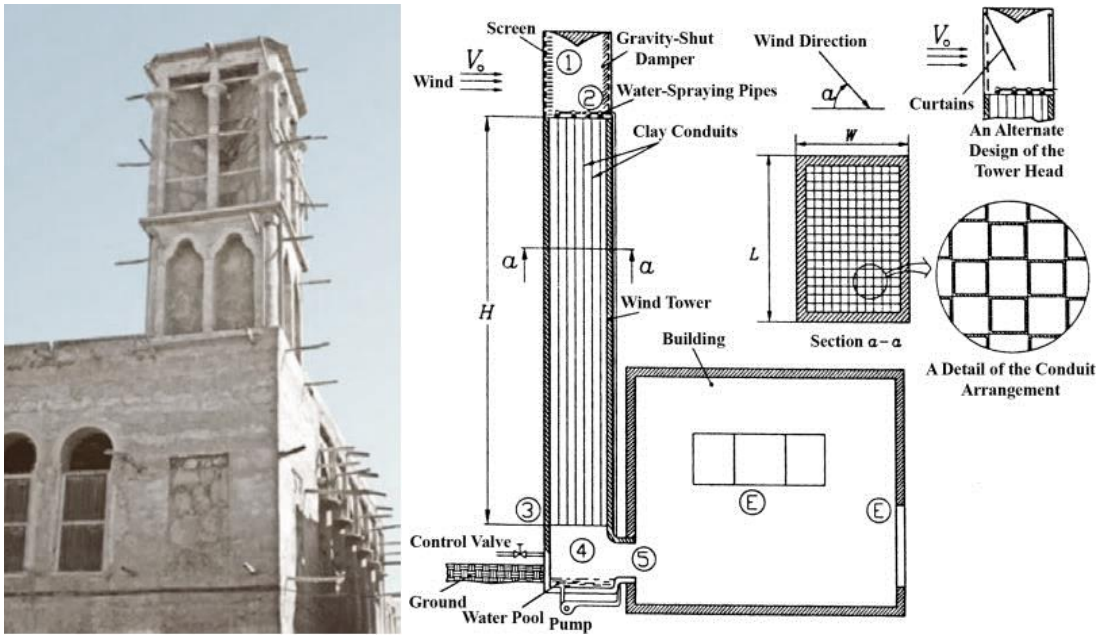

Figure 1 (a) A traditional multi-directional wind tower in the Bastakia area of UAE [13] (b) A traditional wind tower with evaporative cooling proposed by Bahadori [10].

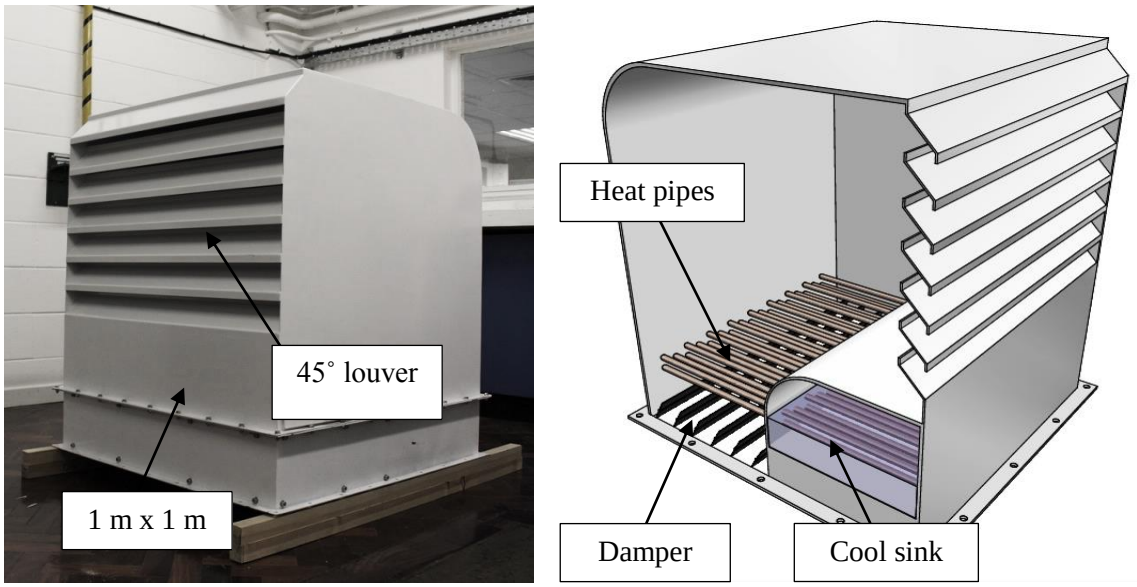

Figure 2 (a) 1:1 scale prototype of the passive cooling windcatcher (b) 3D schematic showing the interior of the system.

Figure 3 Illustrations of "non-functional" wind towers placed on top of buildings in Jumeirah, Dubai, UAE for aesthetic purposes [22].

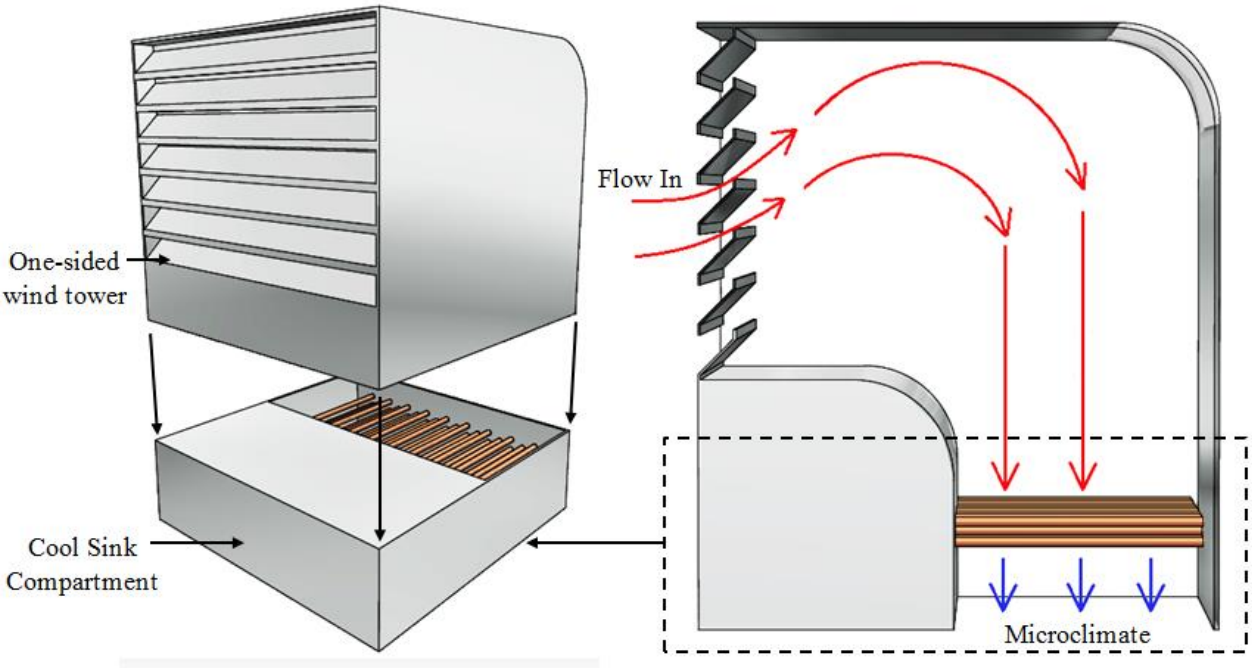

Figure 4 CAD model of the windcatcher with cylindrical heat pipes.

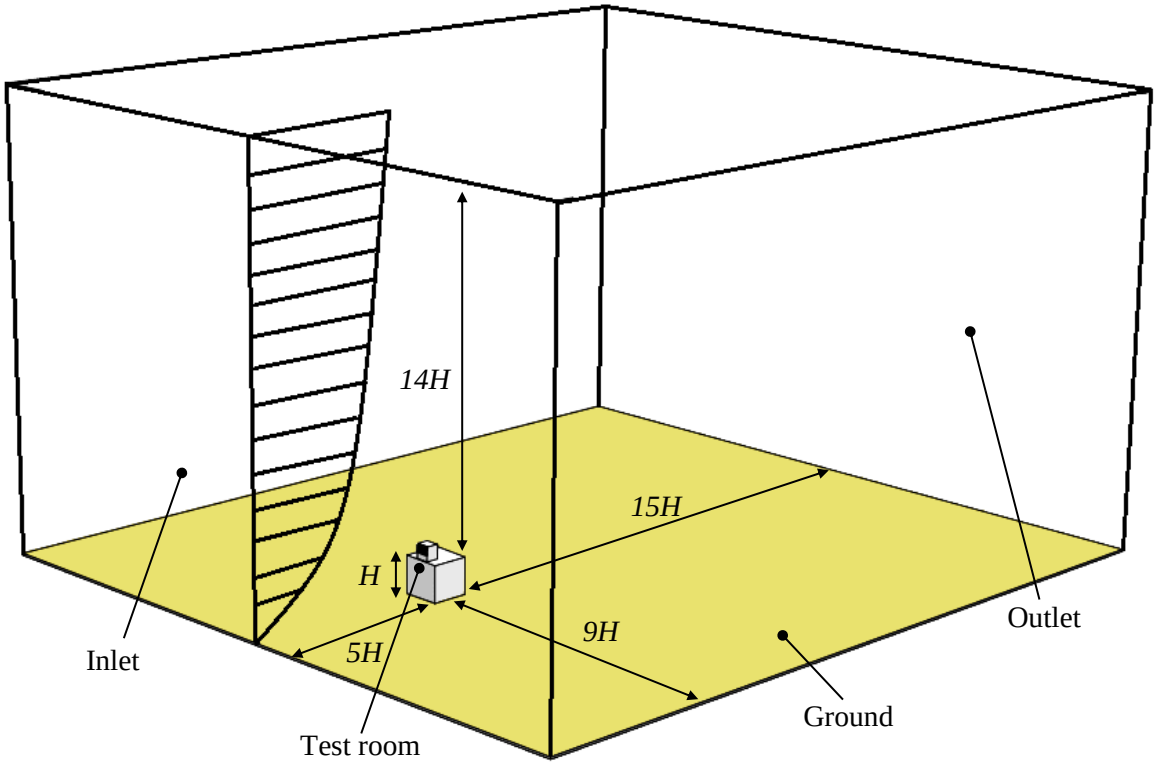

Figure 5 Computational domains for the analysis of the windcatcher.

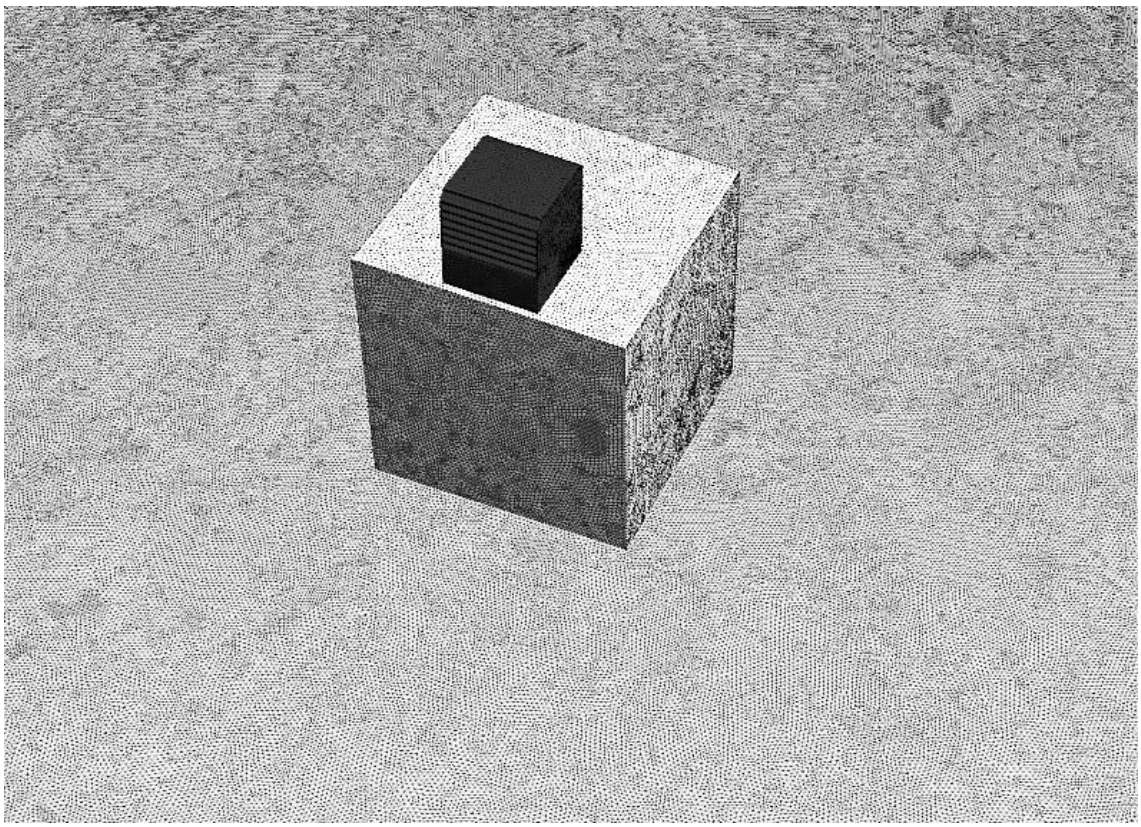

Figure 6 Computational grid of test room with windcatcher.

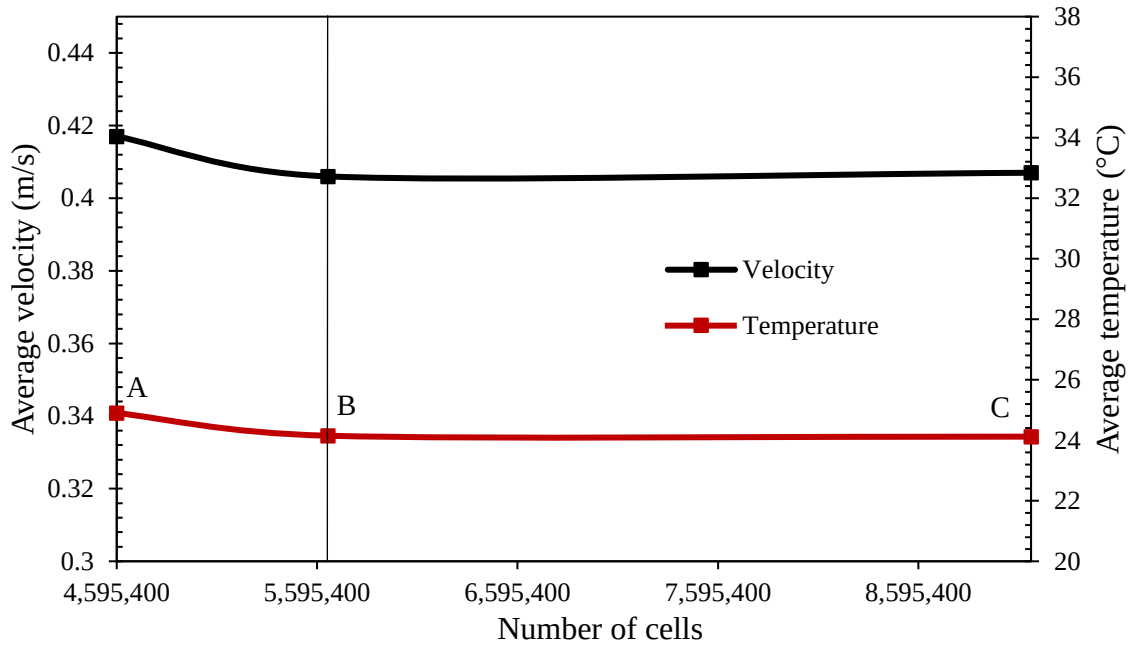

Figure 7 Grid sensitivity analysis of velocity and temperature from 4.59 to 9.16 million cells.

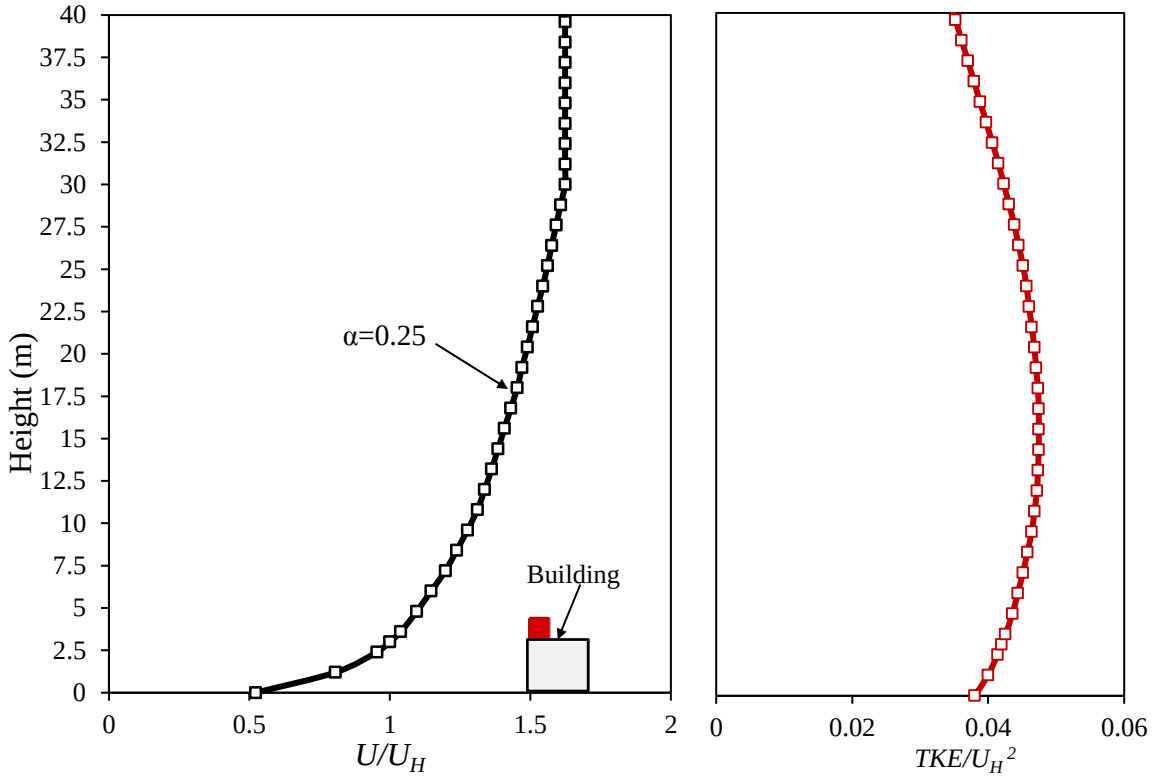

Figure 8 (a) mean stream-wise velocity *U* and (b) Turbulence Kinetic Energy (TKE) *k* of the approaching flow which corresponds to a sub-urban terrain [37F].

(a)

Month of year	Jan	Feb	Mar	Apr	May	Jun	Jul	Aug	Sep	Oct	Nov	Dec	Year
	01	02	03	04	05	06	07	08	09	10	11	12	1-12
Dominant Wind dir.													
Wind probability >= 4 Beaufort (%)	9	27	26	25	27	28	30	37	25	19	18	12	23
Average Wind speed (m/s)	3.6	4.1	4.1	4.1	4.6	4.1	4.6	4.6	4.1	4.1	3.6	3.6	4.1
Average air temp. (°C)	21	23	26	32	36	37	40	39	36	33	27	24	31

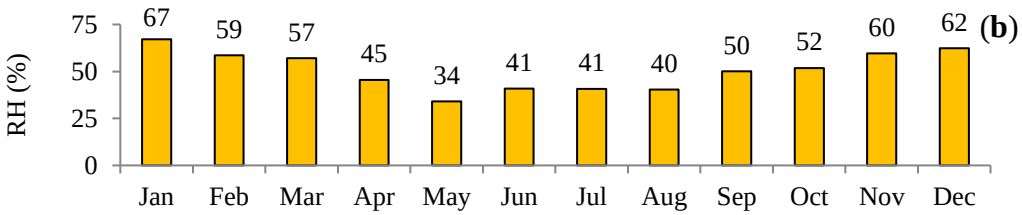

Figure 9 (a) Wind and weather statistics for RAK, UAE (b) mean relative humidity from 06/2013 - 09/2015 [40, 41].

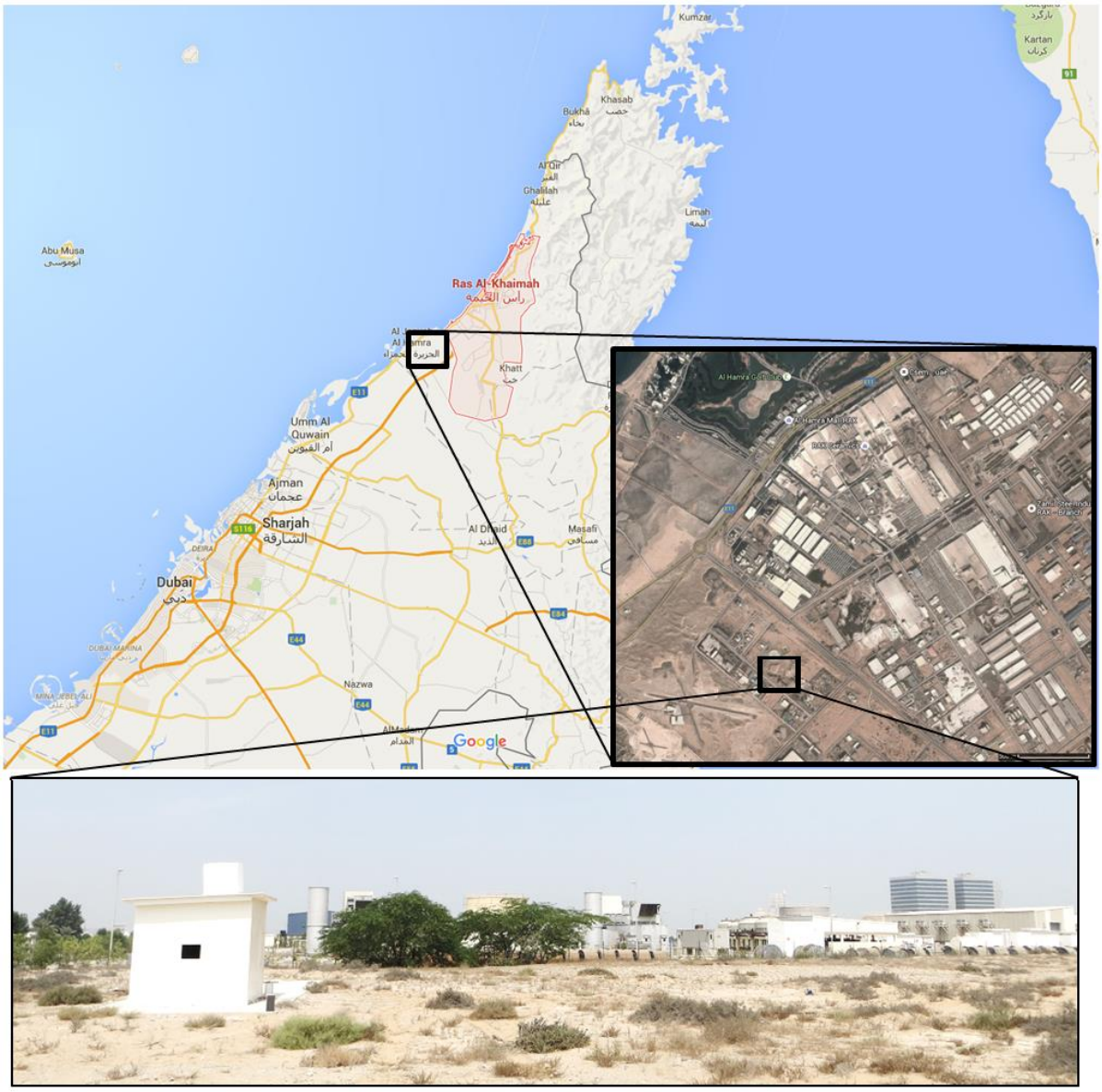

Figure 10 Location of the test site in RAK, UAE.

Figure 11 (a) Isometric view and (b) side view of the windcatcher mounted on top of the test room.

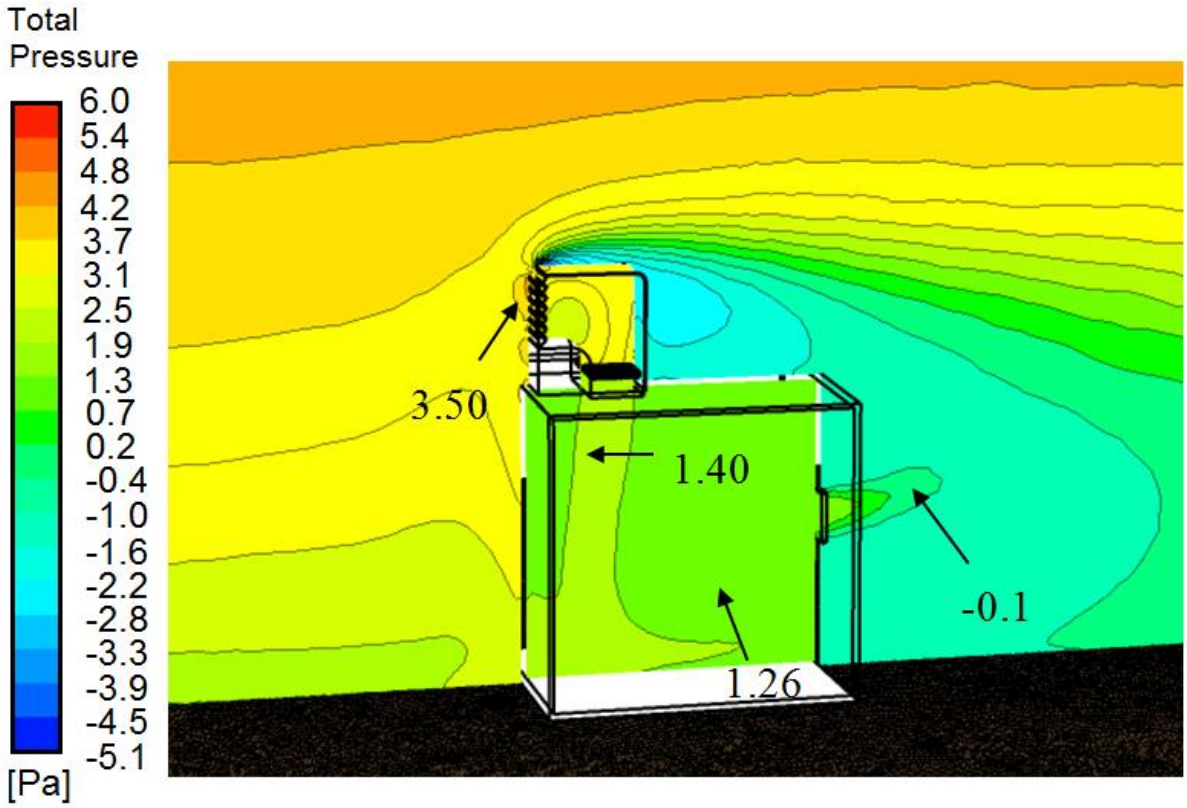

Figure 12 Distribution of the predicted total pressure (P_o).

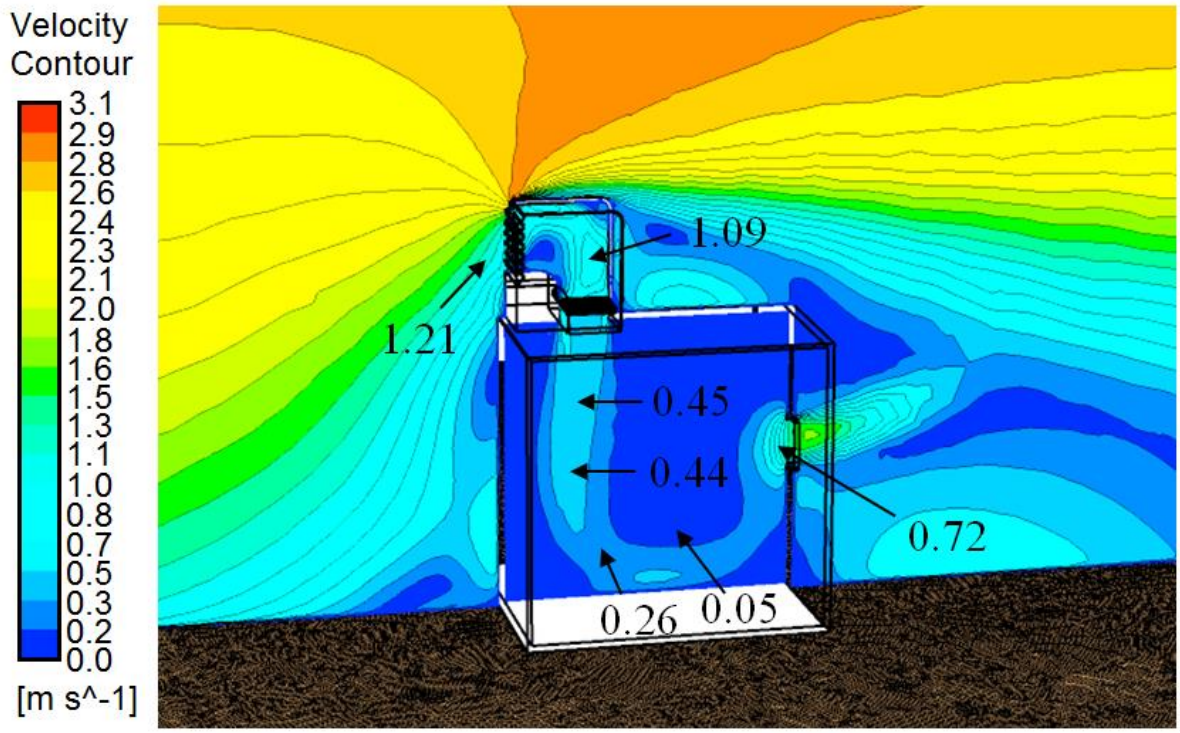

Figure 13 Distribution of the predicted velocity magnitude (m/s) for a windcatcher with heat pipes.

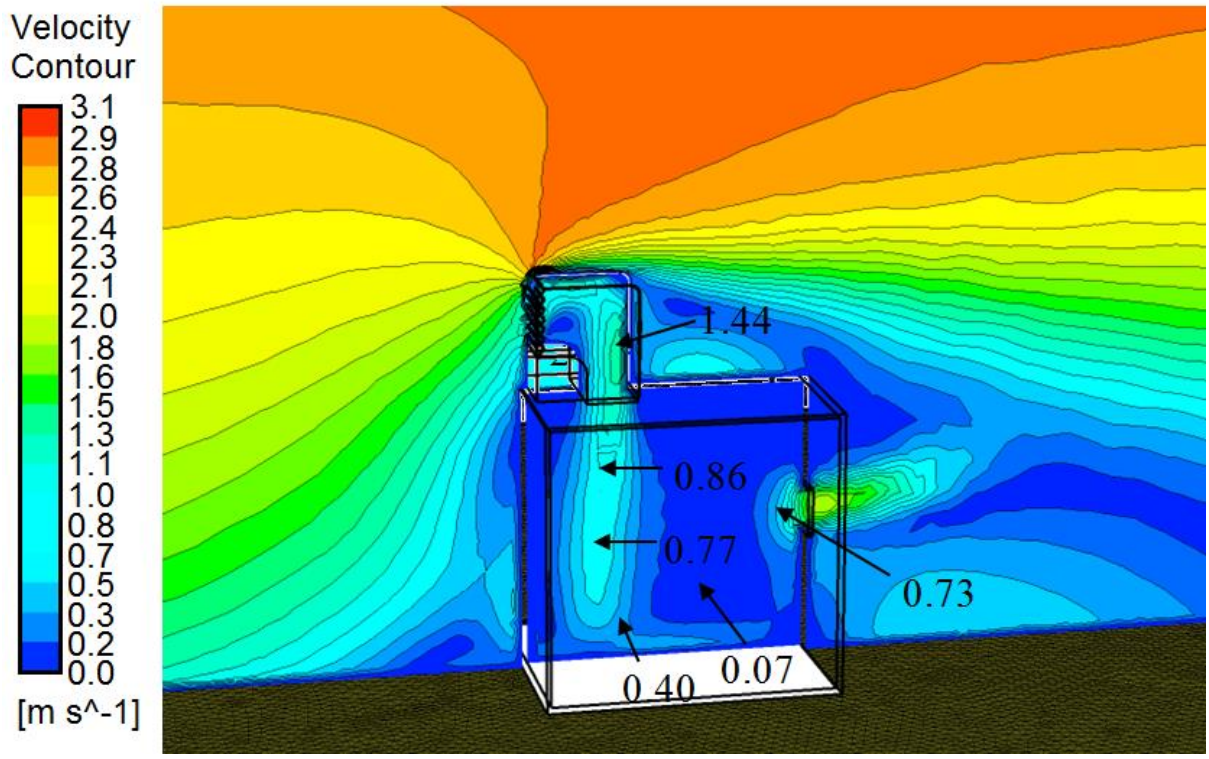

Figure 14 Distribution of the predicted velocity magnitude (m/s) for a windcatcher without heat pipes.

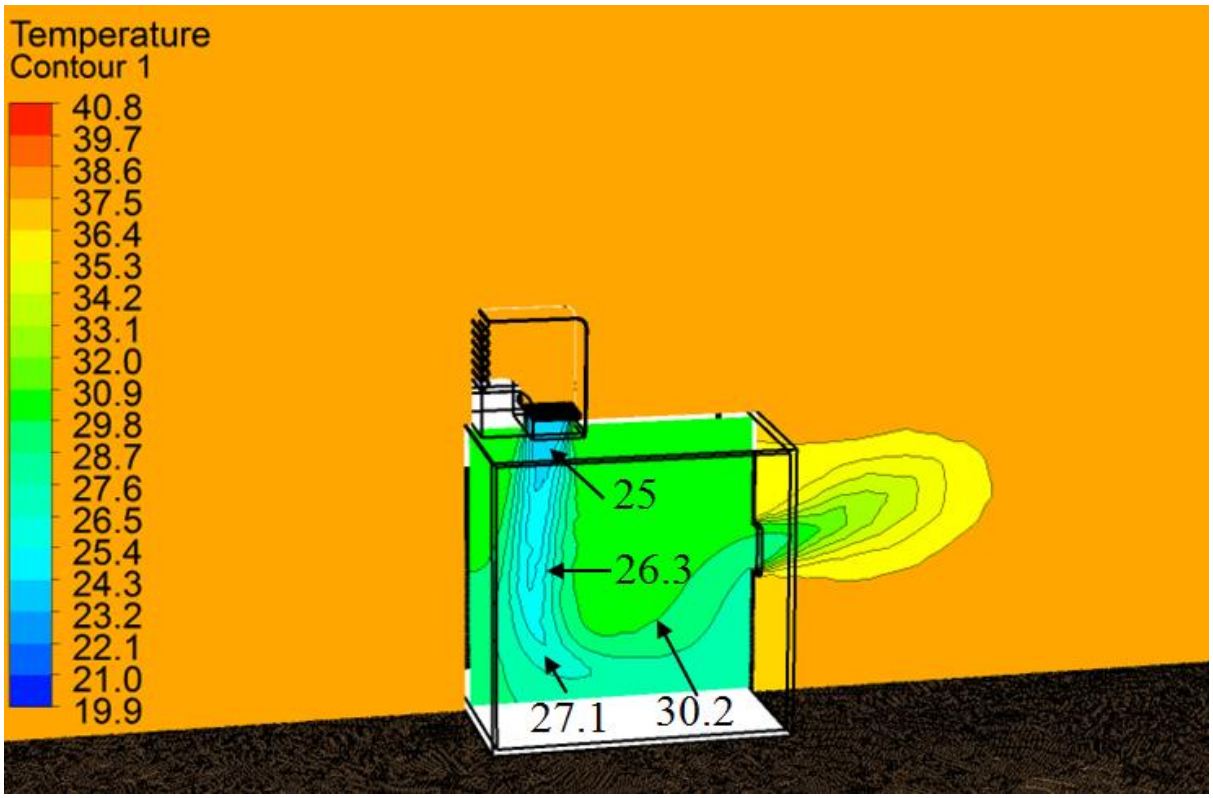

Figure 15 Distribution of the predicted temperature (°C).

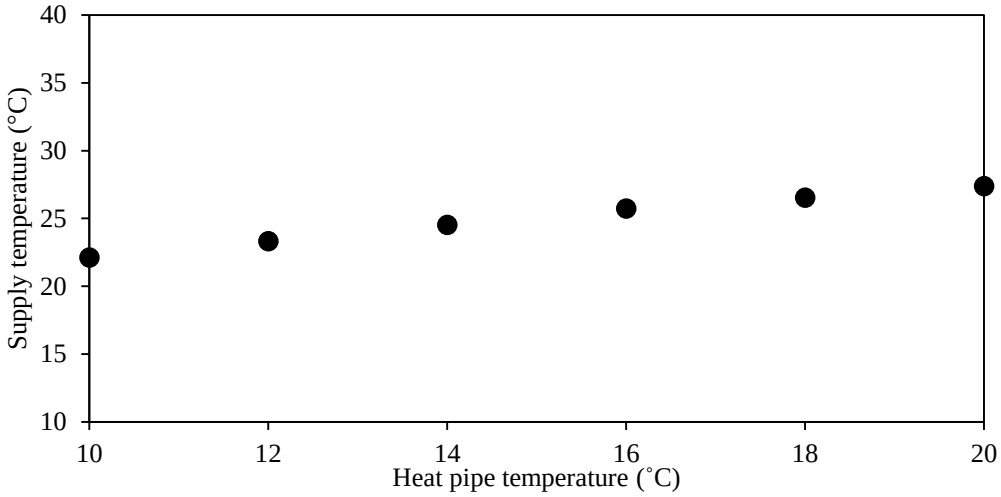

Figure 16 Effect of various heat pipe temperature on thermal performance.

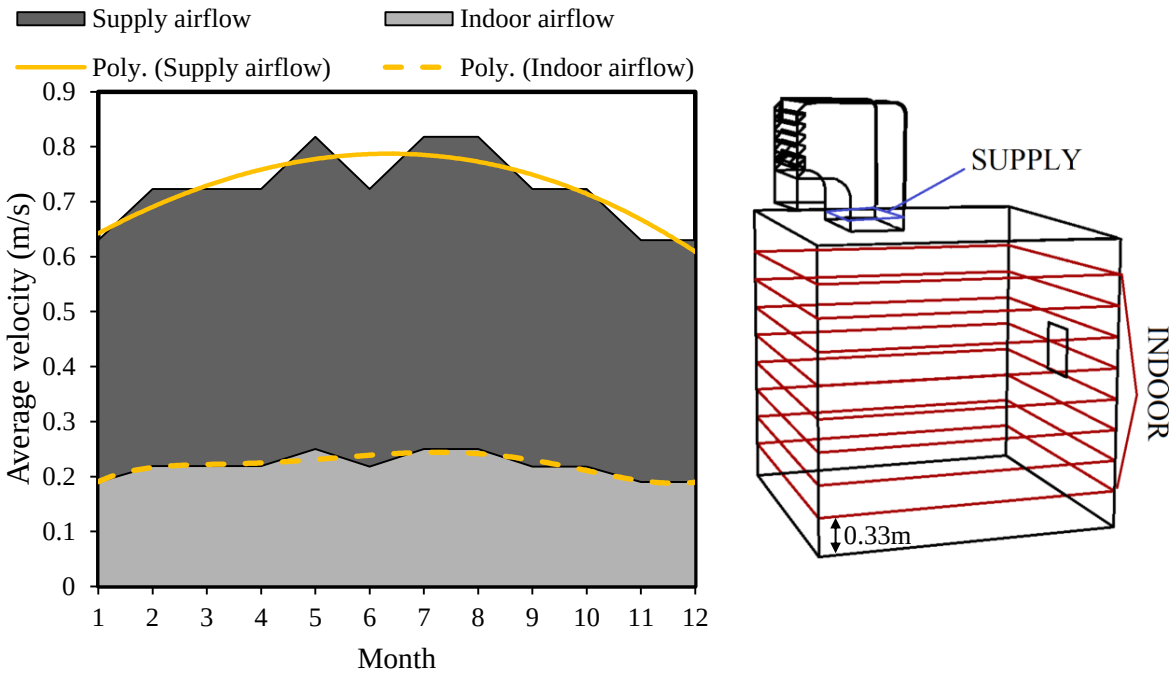

Figure 17 (a) Predicted results for monthly supply and indoor velocity (b) measurement planes for the supply and indoor airflow.

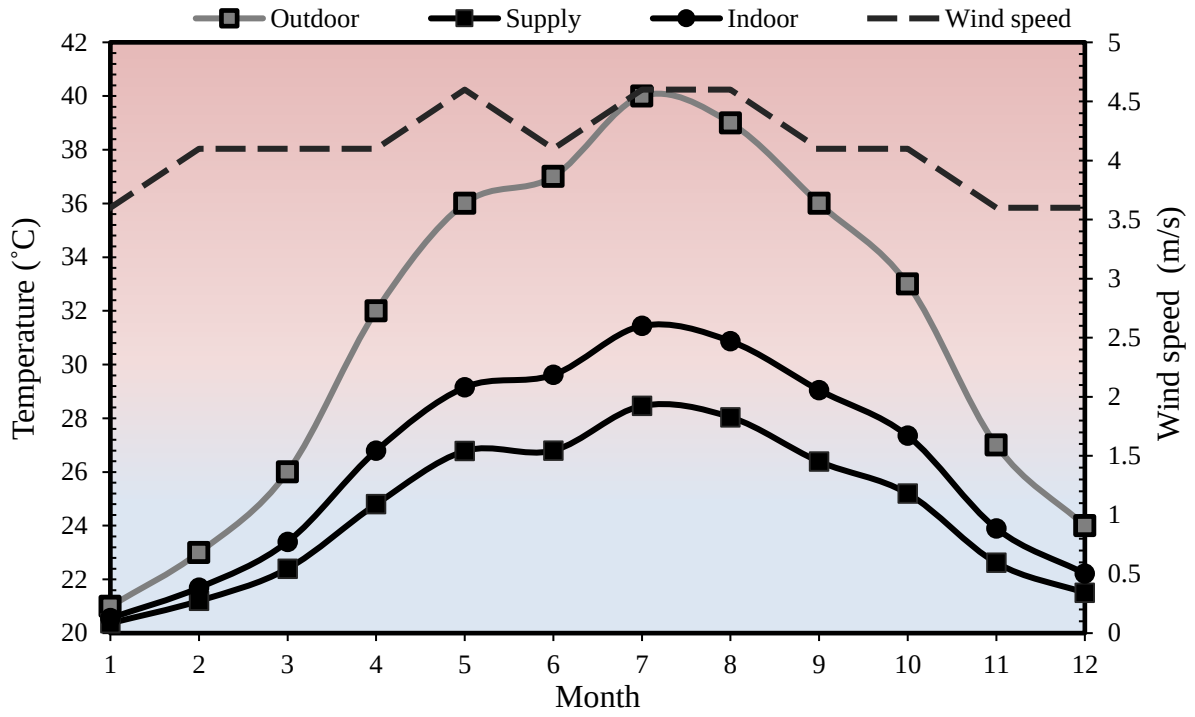

Figure 18 Predicted monthly indoor air temperatures based on RAK weather data. Dashed line represents monthly wind speed (m/s).

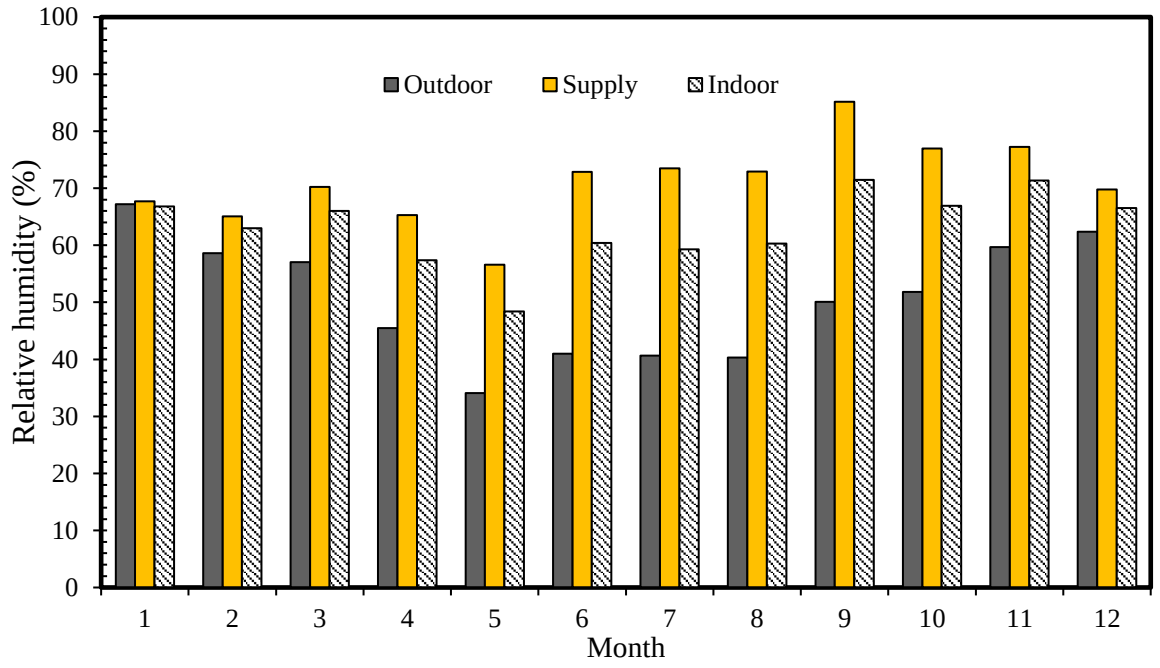

Figure 19 Predicted monthly indoor relative humidity based on RAK weather data.

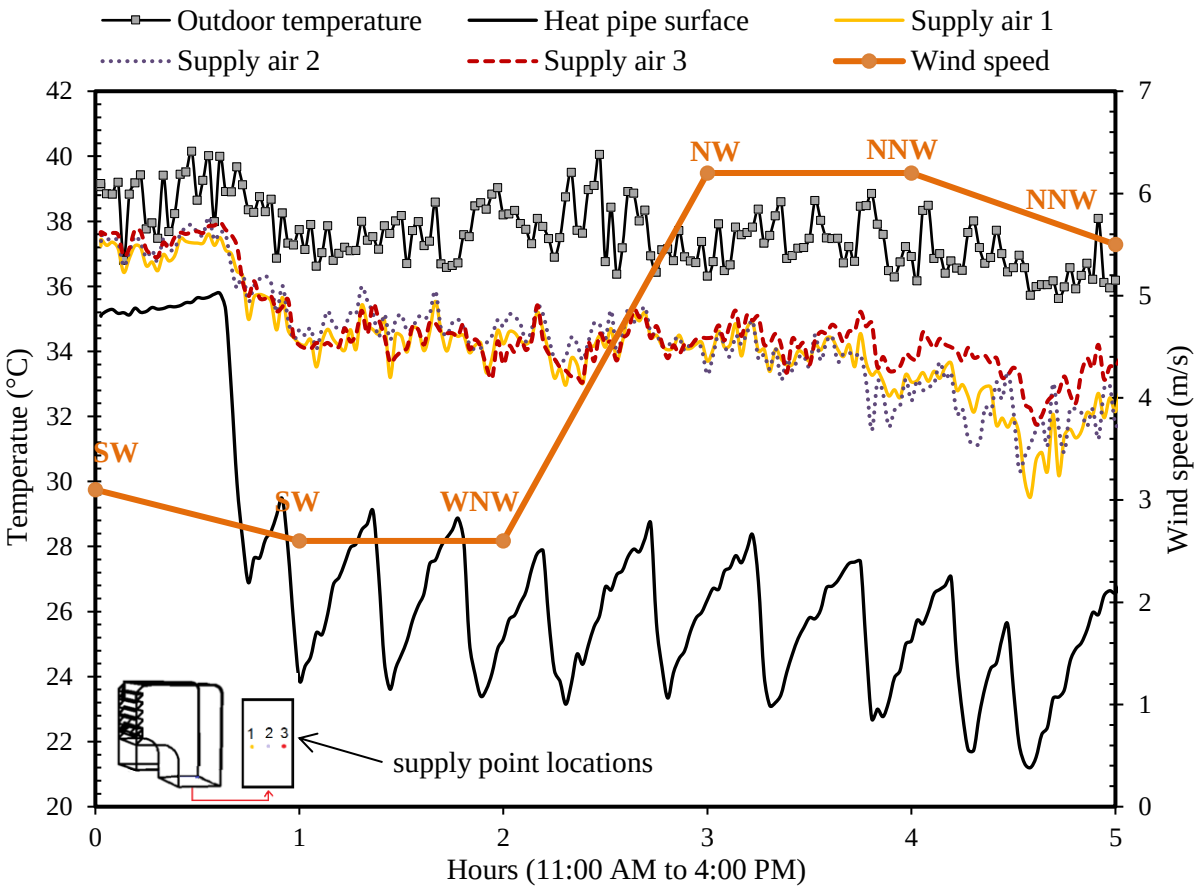

Figure 20 Field testing measurements on 09/17/14.

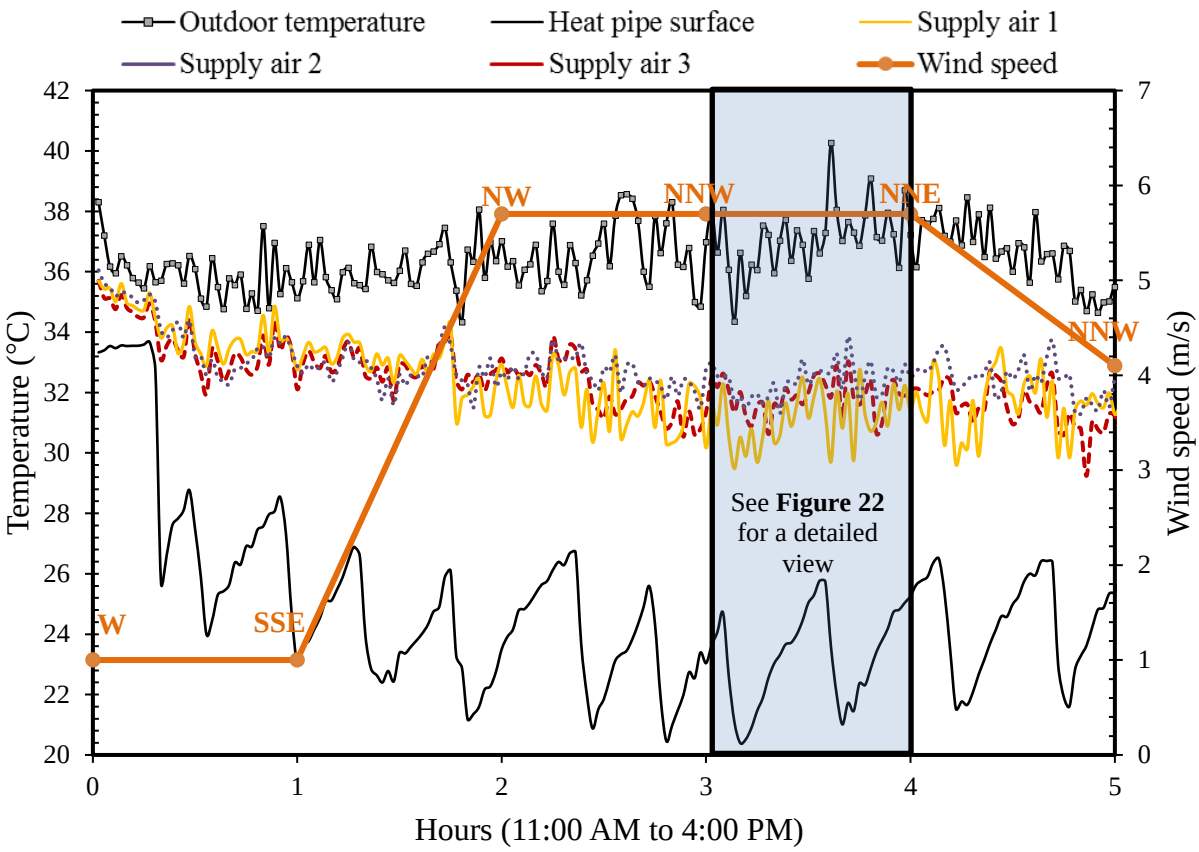

Figure 21 Field testing measurements on 09/18/14.

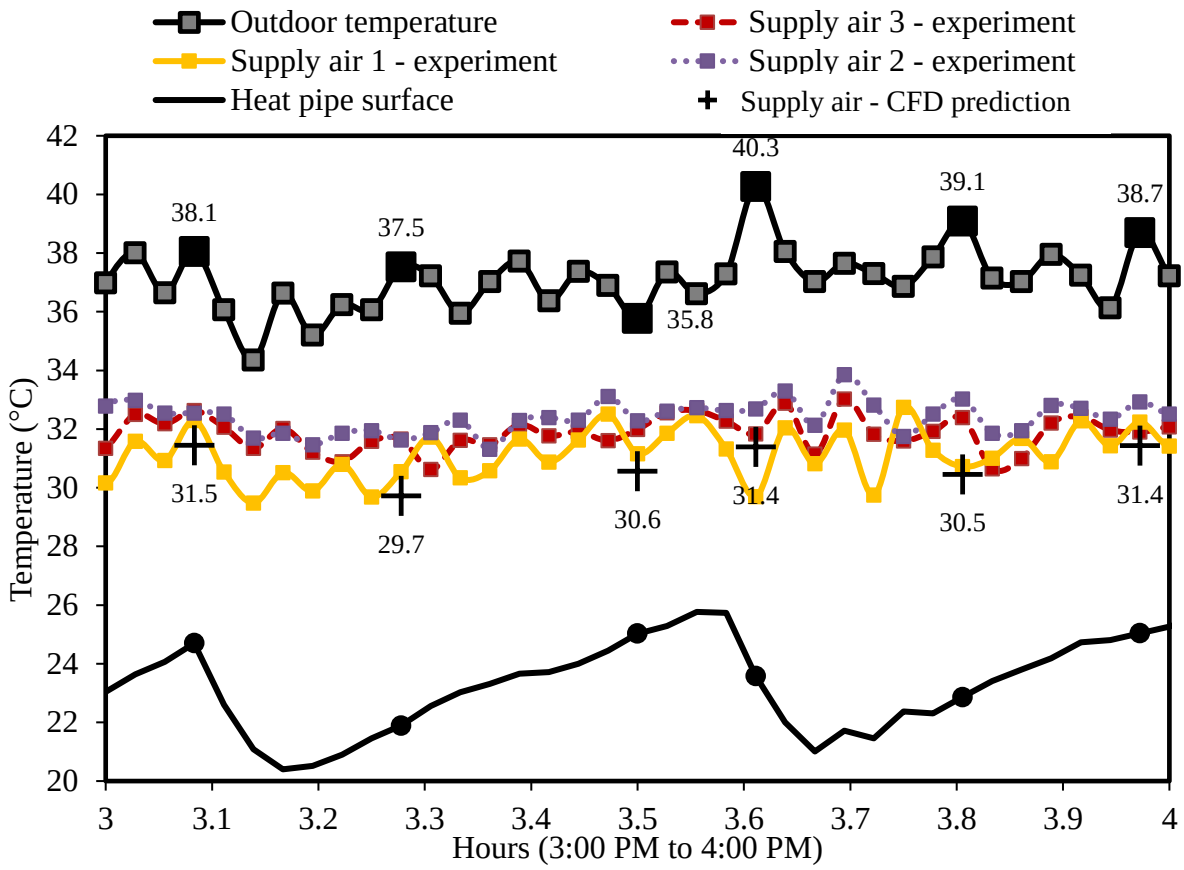

Figure 22 Detailed view of the recorded temperature from 3-4 PM on 09/18/14.

Table 1 Sample calculations of the supply rates of the windcatcher

Month	L/s	L/s/occupant 15 people	L/s/occupant 25 people	L/s/m^2 3 x 3m^2 room	L/s/m^2 6 x 6m^2 room
Jan	315.00	21.00	12.60	35.00	8.75
Feb	361.50	24.10	14.46	40.17	10.04
Mar	361.50	24.10	14.46	40.17	10.04
Apr	361.50	24.10	14.46	40.17	10.04
May	409.00	27.27	16.36	45.44	11.36
Jun	361.50	24.10	14.46	40.17	10.04
Jul	409.00	27.27	16.36	45.44	11.36
Aug	409.00	27.27	16.36	45.44	11.36
Sep	361.50	24.10	14.46	40.17	10.04
Oct	361.50	24.10	14.46	40.17	10.04
Nov	315.00	21.00	12.60	35.00	8.75
Dec	315.00	21.00	12.60	35.00	8.75

Table 2 Comparison between field test data and CFD prediction

Time (PM, GMT +4)	03:05	03:16	03:30	03:37	03:48	03:58
Outdoor velocity [40]	5.70 m/s	5.70 m/s	5.70 m/s	5.70 m/s	5.70 m/s	5.70 m/s
Outdoor temperature	38.05 °C	37.53 °C	35.77 °C	40.27 °C	39.09 °C	38.7 °C
Heat pipe surface temp.	24.7 °C	21.89 °C	25.03 °C	23.58 °C	22.86 °C	25.04 °C
Avg. supply temperature (Actual)	32.55 °C ±0.60 °C	31.09 °C ±0.60 °C	31.72 °C ±0.60 °C	31.41°C ±0.60 °C	32.05 °C ±0.60 °C	32.35 °C ±0.60 °C
Avg. supply temperature (Predicted)	31.50 °C	29.72 °C	30.60 °C	31.39 °C	30.46 °C	31.44 °C
Error	**3.23 %**	**4.41 %**	**3.53 %**	**0.06 %**	**4.95 %**	**2.81 %**